Chemical Physics Letters 812 (2023) 140268

Contents lists available at ScienceDirect

Chemical Physics Letters

journal homepage: www.elsevier.com/locate/cplett

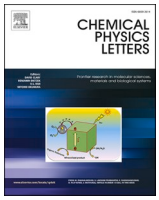

Tracking ultrafast dynamics by sub-20-fs UV pulses generated in the lab open atmosphere

Álvaro Peralta Conde [a], Iker Lamas [b], Marina Sánchez Albaneda [c], Cruz Méndez [c], Asier Longarte [b,*], Raúl Montero [d,*]

[a] Universidad Internacional de la Rioja. UNIR. www.unir.net. Spain
[b] Departamento de Química Física. Universidad del País Vasco (UPV/EHU), Apart. 644, 48080 Bilbao, Spain
[c] Centro de Láseres Pulsados CLPU, Parque Científico, 37185, Villamayor, Salamanca, Spain
[d] SGIker Laser Facility, UPV/EHU. Sarriena, s/n, 48940 Leioa, Spain

ARTICLE INFO

Keywords:
Sub-20 fs UV pulses
Electronic relaxation
Non-adiabatic coupling
Conical intersection
Wavepacket
Electronic coherence

ABSTRACT

This study describes a simple method to generate sub-20 fs UV-pulses (264 nm) by third-harmonic generation, in an air-plasma filament formed after focusing the fundamental 800 nm beam directly in the lab open-atmosphere. The generated pulses are applied to track the relaxation through the conical intersection that couples the S_2 and S_1 states, in the benchmark molecule of naphthalene. The transients, with a resolution of about 25 fs, show two differentiate patterns of quantum beats. The assignation of these oscillations to specific modes in the lower S_1 state and to electronic coherence between the two coupled states is discussed.

1. Introduction

Femtosecond (fs) laser pulses permit to track the evolution of photoexcited molecular systems directly in the time-scale of the movement of their nuclei. Among many other problems, perhaps one of the most natural fields of application has been the description of the non-radiative transitions between non-adiabatically coupled electronic states. Very often, these couplings between the multidimensional electronic potentials are mediated by the presence of conical intersections (CIs) [1,2]. The use of increasingly shorter fs pulses has given access to observables that reflect the interplay between the electronic and nuclear degrees of freedom that occurs in the proximity of these regions.

Going one step further, the unprecedented time-resolution associated to sub-fs laser pulses is making possible to investigate pure electronic dynamics [3,4]. However, the interaction of the extreme peak power and bandwidth carried by attosecond (10^{-18} s) pulses with molecules, produces intricate observables whose interpretation challenges the actual theoretical methodology [5–7]. In this context, pulses with durations around ten or few tens of fs offer remarkable properties for the study of the electronic-nuclear coupling promoted by CIs in molecular systems, in particular:

- They can be tuned to the near part of the UV to explore valence excitations of neutral molecules.
- While they provide enough energy resolution to induce individual targeted excitations, they carry the required bandwidth to efficiently prepare wave-packets that can travel through the coupling regions.
- The pump–probe schemes based in pulses of these durations provide temporal resolutions of few fs.

Numerous studies employing different pump–probe techniques have demonstrated these ideas by recording time-dependent signals that reveal the relaxation dynamics through CIs, with resolutions of few tens of femtoseconds. While initially, these methods were applied to gas phase molecules detected by ionization [8–11], they have been successfully extended to molecules in solution by using techniques based in optic detection [12–15]. In parallel, the development of theoretical models have permitted the interpretation of the recorded observables, which in general reflect a combination of the change in the electronic character and the involved nuclear wave-packet dynamics [16–21].

Herein, we report on the generation of sub-20 fs pulses at 264 nm, which are used for time-resolved ionization (TRI) measurements. The conducted experiments explore a simple method to tune the fundamental 800 nm beam to the UV by producing the third harmonic (TH) directly in air at atmospheric pressure. The applied method has allowed

* Corresponding authors.
E-mail addresses: asier.longarte@ehu.es (A. Longarte), raul.montero@ehu.es (R. Montero).

https://doi.org/10.1016/j.cplett.2022.140268
Received 25 October 2022; Received in revised form 5 December 2022; Accepted 13 December 2022
Available online 15 December 2022

us to investigate the internal conversion (IC) between the S_2 and S_1 states of naphthalene, with resolutions in the order of 25 fs. The weak S_0–$S_1(L_b)$ transition, with origin at 32020 cm^{-1} (3.97 eV), is polarized along the long axis of the molecule, while the S_0–$S_2(L_a)$ with much higher oscillator strength, is located at about 35900 cm^{-1} (4.45 eV) and mainly polarized along the short axis.

According to previous studies, it is well established that the interaction between these two electronic configurations controls the photophysics of naphthalene after excitation in the lower portion of the UV absorption [22–24]. Furthermore, the two involved states, the higher bright S_2 (L_a) and the lower dark S_2 (L_b), represent a structure of valence coupled ππ* excitations common to molecules containing aromatic chromophores. In addition, naphthalene offers a highly symmetric rigid structure that, as in the extensively studied case of pyrazine [9,25,26], permits to relate the recorded observables with the vibrational modes involved. All this makes naphthalene a good case study to explore the potential of the generated short femtosecond pulses for the study of non-adiabatic dynamics through CIs, which is confirmed by the novel information contained in the recorded observables.

2. Methods

2.1. Experimental

In order to carry out the reported TRI measurements, a new experimental set-up was built at the Pulse Laser Centre (CLPU) laboratories in Salamanca (Fig. 1). Femtosecond laser pulses were generated by a FEMTOLASERS (FemtoPower Compact PRO CEP) laser system. This source produced a 1 KHz train of 25 fs pulses centered at 800 nm with ~2 mJ. After reducing the energy to 0.75 mJ by taking the central portion of the beam with a circular aperture (Ø=1 cm), the beam was divided in two branches by means of a fused silica beam splitter. The transmitted part was used for pumping the UV generation, while the reflected one served as probe. A negative chirp (-325 fs^2) was introduced in the initial pulse to compensate for the dispersion induced by the beam-splitter. For the probe beam, the 130 μJ reflected portion was introduced directly into the beam manipulation chamber (Fig. 1). The energy of the probe beam is further reduced to 30 μJ by a second aperture prior entering the manipulation chamber to reach the appropriate ionization regimen. The pump beam was obtained by focusing about 530 μJ of the fundamental beam in the lab open atmosphere (T = 20 °C, H = 40 %) by a 300 mm focal spherical mirror. The TH of the fundamental was generated in the formed air-plasma filament [27,28]. Size, energy and focusing conditions of the incident fundamental beam were carefully adjusted to optimize the generation of the TH. In optimum conditions, about 110 nJ of TH were generated. The emergent TH beam was characterized spectrally (Fig. 2), yielding bandwidths compatible with ~13 fs durations (see below for further consideration on the temporal resolution achieved). We should mention that the achieved stability of the UV pulse intensity was about 4 % (standard deviation), even without taking any precaution to protect the filament from airflows in the lab.

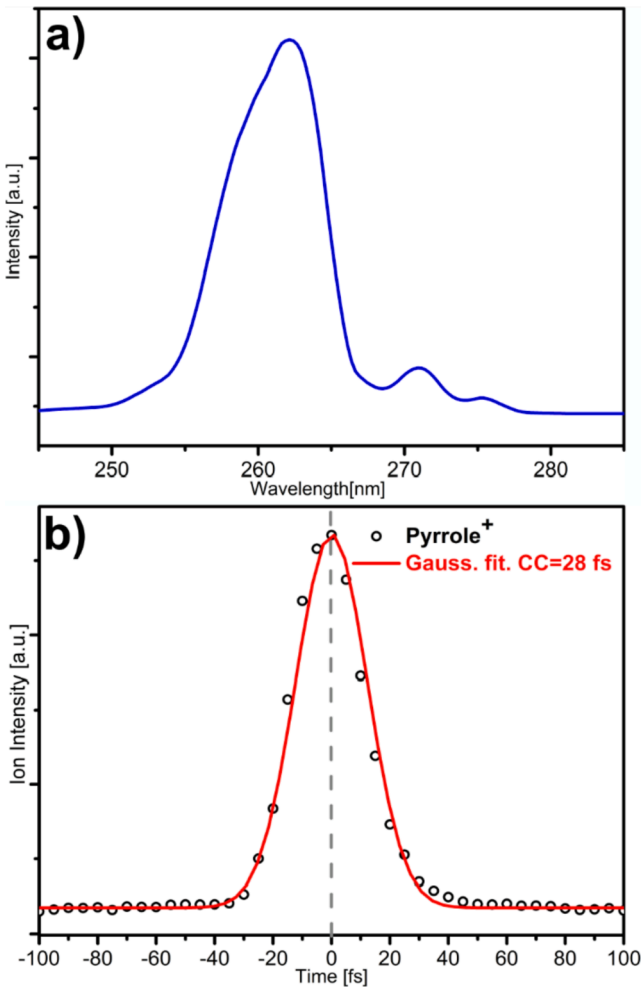

Fig. 2. a) Spectrum of the 3ω generated from the air-plasma filament formed in the open atmosphere of the lab. The ~12 nm bandwidth is compatible with ~13 fs durations. b) The dots are the pump–probe 1 + 3′ non-resonant ionization signal of pyrrole. The Gaussian fit (red line) yields a 28 fs FWHM value.

In order to deliver the TH pump beam to the ionization region of the

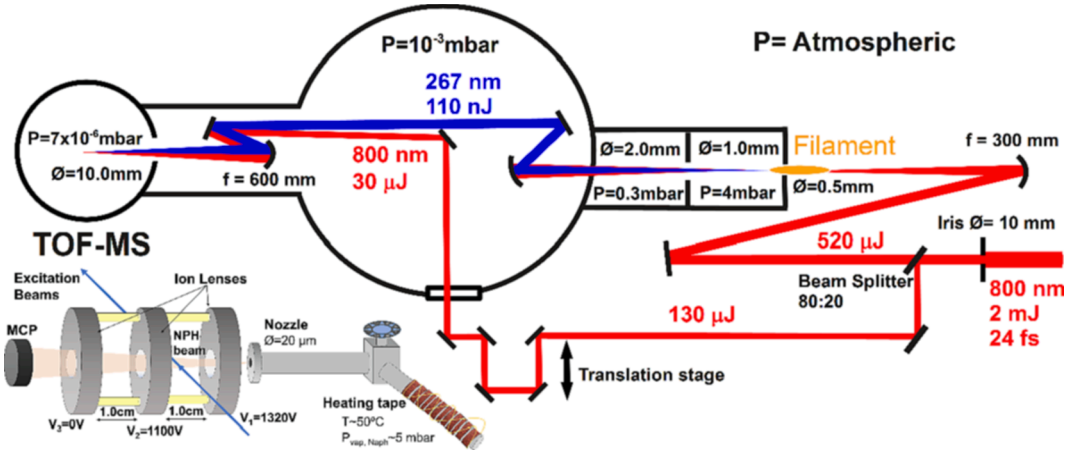

Fig. 1. Scheme of the experimental set-up built for the time resolved ionization measurements. The inset shows a detailed view of the mass spectrometer.

TOF mass spectrometer, avoiding the dispersion caused by any transmissive optics, a differential pumping system that drops the pressure from atmospheric to the $7x10^{-6}$ mbar of the interaction region, was employed. This system consists of three differentially pumped chambers separated by apertures of increasing size, as indicated in Fig. 1. The first 500 μm diameter aperture was placed at the end of the filament generated by the focused incident beam, allowing the generated TH to enter the first chamber. The two subsequent apertures permitted to transfer directly the TH beam to the manipulation chamber. There, it was collimated by a 300 mm focal length UV-enhanced aluminum mirror, filtered by two reflections on low GDD (10 fs^2) dielectric mirrors and finally focused, together with the fundamental probe that entered the chamber through a 3 mm fused silica window, into the ionization region by a 600 mm focal spherical mirror. With this simple geometry, the angle formed by the non-collinear beams at the interaction region was kept low enough to guarantee a good overlap and avoid degradation of the temporal resolution. Typically, the pump and probe reached in the ionization region intensities in the order of 10^9 and 10^{11} W/cm^2, respectively.

The homemade mass spectrometer was equipped with an ionization region formed by three electrostatic lenses according to the design by Eppink and Parker (Fig. 1) [29]. The formed ions were focused into a dual MCP detector located at the end of a 30 cm flight tube. The vapor pressures of the solid naphthalene and pyrrole, increased by a heating system, were mixed with 0.5 atm of He and expanded through a 20 μm nozzle to form an continuous molecular beam. A vacuum system based in a 1000 l/s turbomolecular pump permitted to maintain pressures $\sim 4x10^{-5}$ mbar in the ionization region, when the molecular beam was operated.

The ion spectra were monitored by a digital scope, while the signals of the masses of interest were integrated and subsequently stored in a PC computer for their analysis. The acquisition software also controls the position of a linear translation stage (Thorlabs Z825) that permits to adjust the pump–probe delay pathway with ~1 fs precision.

In order to test the temporal resolution of the system and to establish the zero-delay reference during the naphthalene time-dependent measurements, the 1(264 nm) + 3′(800 nm) non-resonant ionization signal of pyrrole (Py^+) was employed. It has been firmly established that the pyrrole molecule is non-resonantly ionized in this process [30,31]. Fig. 2 shows the instrumental response function recorded by this method, which yields a value of 28 fs for the signal FWHM. It is worth to remark here that, as indicated above, in order to compensate the dispersion in the pump beam, a negative GDD (-325 fs^2) was introduced at the compressor stage so that the NIR pulses are Fourier transform limited at the UV generation point. However, as the probe pulses propagate through less material (3 mm of fused silica) it carries a small residual chirp (-220 fs^2) corresponding to ~35 fs. Knowing this value and the order of the ionization process of pyrrole signal 1(267 nm) + 3′(800 nm), from the measured cross-correlation (ω_{IRF} = 28 fs) it is possible, by applying the following expression [32],

$$\omega_{IRF} = \sqrt{{\omega_{pump}}^2 + {\omega_{probe}}^2/n} \quad (1)$$

to derive the duration of the generated UV pulse, which yields a value of ~19 fs. This number is close to its Fourier transform limit of 13 fs. Then, a proper compensation of the GDD in both branches could provide a potential time resolution of ~23 fs.

2.2. Computational

In order to elucidate the nature of the electronic states and the vibrational coordinates involved in the recorded transient signals, TD-DFT calculations were carried out by Gaussian 16 software package [33]. In all cases the CAM-B3LYP functional with the 6–31++G** basis set was used. In this work, the Mulliken[34] convention for the D_{2h} point group, with yz as the molecular plane, will be used. First, vertical excitations from the optimized S_0 (A_g) geometry to the $S_1(B_{2U})$ and S_2 (B_{1U}) states were calculated. Then, the minima of the S_1 and S_2 states were optimized and their harmonic vibrational frequencies obtained. Unrelaxed energy scans along selected vibrational coordinates, starting at the S_0 minimum, were also carried out for the S_0, S_1, S_2, D_0 (^2A_u) and D_1 ($^2B_{3u}$) states.

3. Results and discussion

Fig. 3a shows a 1(264 nm) + 3′(800 nm) TRI decay that accounts for the total ionization signal recorded at the Naphthalene$^+$ mass channel as function of the pump–probe delay. In principle, the signal resembles that registered by previous TRI experiments at similar excitation wavelengths [23,24], but using longer pulses in the 60–100 fs range. As it is analyzed in detail there, the recorded transient is composed by a first ~40 fs decay followed by a constant background that reflects the IC of the initially prepared $S_2(L_a)$ state to the lower long-living (ns) $S_1(L_b)$ state. The vertical excitation at 264 nm prepares the naphthalene molecule in the $S_2(L_a)$ excited state, whose absorption onset has been calculated at 36800 cm^{-1} (4.56 eV) [35,36], in good agreement with the experimental detection at 35900 cm^{-1} [23,26]. The lower $S_1(L_b)$ carries no oscillator strength, although it can be weakly induced by vibronic coupling, mainly with S_3. Its origin is located at 32020 cm^{-1} (3.97 eV) and predicted at 32500 cm^{-1} (4.03 eV) [35–37]. In this situation, we can assume that the pump pulse prepares a wavepacket exclusively on the S_2 surface.

However, in comparison with previously recorded transients [23,24], the signal In Fig. 3a shows more complex oscillations that are more clearly perceptible in Fig. 3b, where the exponential fit (red trace in Fig. 3a) has been subtracted. The remaining trace shows an oscillatory pattern formed by quantum beats with at least two different periods. By taking the Fourier transform of the full-length signal (Fig. 3c), we find two frequencies with periods of 289 ± 91 and 59 ± 4 fs that correspond to 115 ± 36 and 565 ± 27 cm^{-1} energies, respectively. It is worth to note that the slower contribution had already been detected in previous experiments [24], while the observation of the faster beating has to be attributed to the shorter pulses applied in the present experiments. More precisely, the appearance of the fast beating could be related to two associated effects: i) the improved temporal resolution that allows us to resolve the maxima separated by 59 fs. ii) the larger bandwidth of the excitation pulses (~772 cm^{-1}), which makes possible to form a wavepacket that encompasses at least two vibrational levels of the prepared $S_2(L_a)$ state (see below for an extended explanation).

A rigorous modelling of the recorded transient is beyond our actual capabilities and out of the scope of the present manuscript. However, by assigning the observed oscillations with the help of simple calculations and previous theoretical and experimental data, we can infer some novel relevant aspects of the relaxation followed by the system, which involves the non-adiabatic $S_2(L_a)/S_1(L_b)$ coupling. The non-adiabatic coupling between the S_2 and S_1 states of naphthalene has been spectrally characterized in previous studies [37,38], while more recently, as mentioned above, the ultrafast IC from the initially prepared S_2 to the lower S_1 has been tracked by time-resolved photoelectron and photoion measurements [22–24]. Despite this, to the best of our knowledge, and on the contrary to the naphthalene cation [39,40], there is no description of the S_2/S_1 coupling in terms of CIs.

The carried out calculations place the $S_0 \rightarrow S_1$ (L_b, B_{2U}) and $S_0 \rightarrow S_2$ (L_a, B_{1U}) vertical excitations at 4.66 (266.04) and 4.73 eV (262.12 nm). Although the values are clearly overestimated respect to the experimental ones [37] and higher level calculations [35,36], the involved molecular orbitals are those previously described (Fig. 4a). From the S_2 and S_1 vertical geometries the minima of the states were optimized. The optimization of the S_2 state easily takes the system to a minimum at 4.25 eV, which, at this calculation level, becomes the global excited state minimum. On the other hand, in order to reach a minimum on S_1, it is required to walk the system along the ν_8 B_{3g} coordinate (according to the

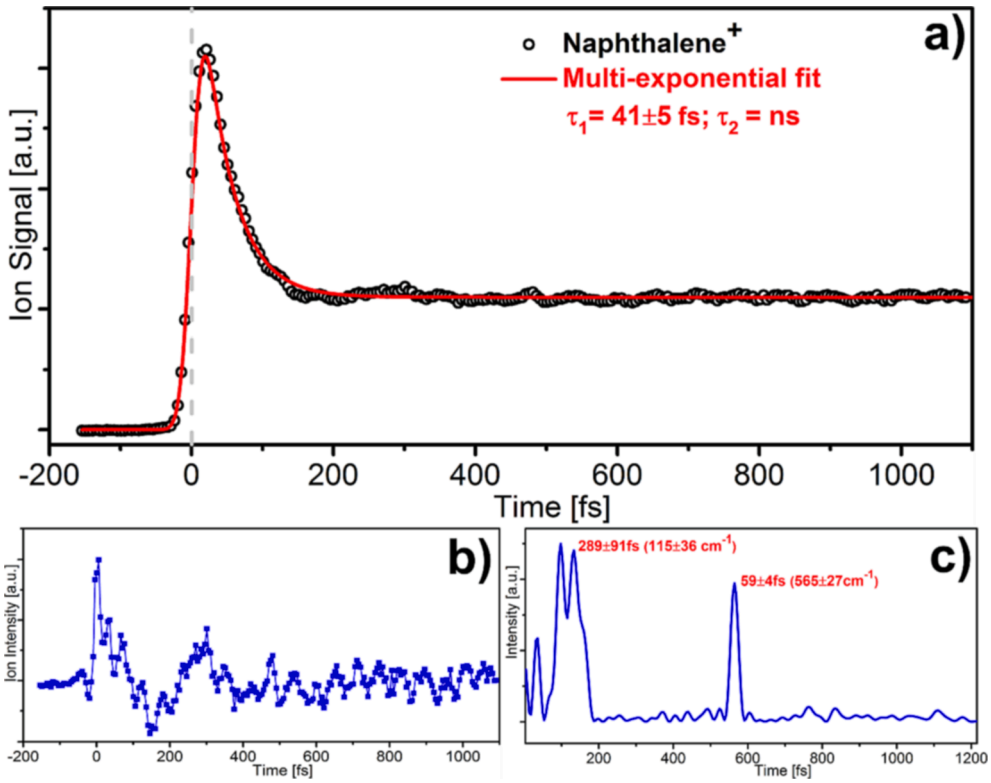

Fig. 3. a) The dots correspond to the 1(264) + 3′(800) pump/probe signal recorded at the naphthalene$^+$ channel. The solid red line is the best multi-exponential fit obtained. b) Oscillatory portion of the transient shown in a) obtained after subtracting the exponential fit (red line). c) FFT spectrum of the oscillatory signal shown in b).

nomenclature employed in Refs. [37,41]), a skeletal distortion of the ring on the molecular plane. The harmonic frequency for this S_1 vibration is calculated at 458 cm^{-1} (same value for S_2) and experimentally observed at 435 cm^{-1} in the fluorescence excitation spectra [37,42]. Along this mode, the minimum reached is substantially the same location on the L_a surface obtained from the S_2 optimization, but has a lower C_{2h} symmetry. Although the TD-DFT can not offer a proper description of the non-adiabatic coupling, the optimizations of the S_2 and S_1 states permit to infer that both surfaces cross to form a CI. As the ν_8 B_{3g} vibration has the right symmetry to couple the B_{2U} and B_{1U} states, it is very likely-one of the modes responsible of the coupling of the S_2 and S_1 surfaces.

Grounded on this picture of the S_2 and S_1 states we can try to interpret the measured transients, in particular, the oscillations. The excitation at 267 nm prepares the molecule in the $S_2(L_a)$ excited state, with a vibrational content of about 1500 cm^{-1}. According to previous dynamic measurements and the present data, the initially prepared state relaxes with a ~40 fs lifetime [22–24], as it is shown by the initial decay Fig. 3a transient. The formed S_1 state relaxes in the ns time scale [37,43], which is reflected by the remaining ionization signal recorded during the full observation window. Regarding the periodic beatings, in principle they should have a vibrational origin. However, their assignation to the corresponding modes is far to be straightforward, as we expose in the following discussion.

We consider first the fast 59 fs (565 cm^{-1}) period beating. It is tracked for delays longer than 1 ps, up to the limit of the observation window. At these long delays, after the decay of the initially excited S_2 state, only the lower S_1 diabatic state (or the lower adiabatic S_2/S_1 surface) remains populated and consequently, the observed wavepacket activity has to occur on it. Here, it is important to note that the frequency of the two beatings have been extracted for the full observation window, from the onset of the S_2 state to the limit of the detection. However, a Fourier analysis by considering shorter windows, in particular, after suppressing the earlier part of the signal, have not yielded substantially different frequency values. In this situation, it is not clear if the observed wavepacket is formed in the S_2 state prepared by laser-coupling to the ground state and then transferred to the S_1 or alternatively, directly induced in the S_1 state by the non-adiabatic coupling with the S_2 state. Even so, in either case, the assignation can be based on the S_1 state vibrational frequencies. Assuming that the wavepacket is induced by the S_2/S_1 coupling, in principle, some good candidates for the modes showing vibrational activity are the tuning modes involved in the CI, along which the S_2 and S_1 minima are shifted. Indeed, in a closely related system with the same symmetry, as the $S_2(\pi\pi^*)/S_1(n\pi^*)$ CI of pyrazine, the observed oscillations on the lower surface have been assigned to the ν_{6a} tuning mode [25]. For naphthalene, the A_g tuning vibrations are also the modes active in the S_1-S_0 transition, since the fluorescence excitation spectrum recorded in jets can be used to identify the S_1 frequencies [37]. The lowest A_g fundamentals are observed at 501, 700, 984 and 1143 cm^{-1}, which correspond to the 485, 715, 1020 and 1137 cm^{-1} calculated harmonic frequencies [42].

Among these frequencies, the 700 cm^{-1} vibration, assigned to a deformation of the naphthalene rings (ν_8 A_g in Refs. [37,41]), could be more likely the mode responsible of the measured 565 cm^{-1} oscillation. As expected, the unrelaxed energy scans along this mode (Fig. 4b), show that the S_2 and S_1 surfaces cross. The fact that this transition between the S_1 origin and the first level of the ν_8 A_g vibration appears at a substantially higher value can be attributed to the expected anharmonicity of the potential. In particular, considering the vibrational content of about 5859 cm^{-1} in the formed S_1 state, the observed wavepacket could reflect one quanta differences between higher vibrational levels.

The observability is another key aspect when assigning the measured beating, which depends on the modulation of the ionization cross-section along the considered vibration. In general, a vibration will be observed if the PES of the excited state along this coordinate is not parallel to that of the ion, or in the case of multiphoton ionization, to

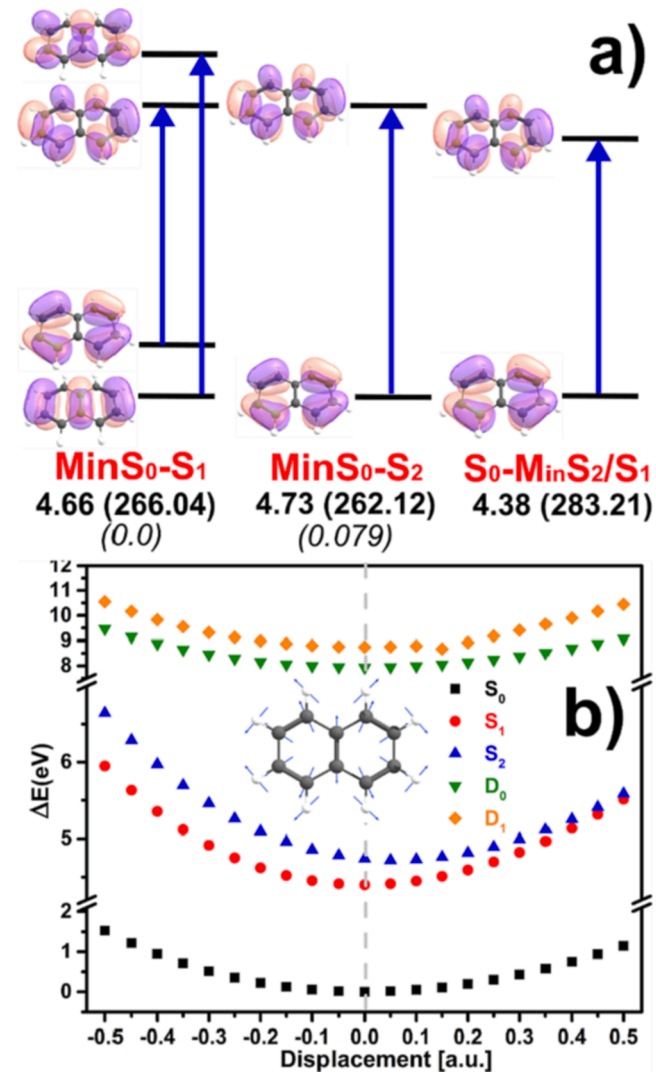

Fig. 4. a) Energies in eV (nm), oscillator strengths (cursive) and molecular orbitals calculated (TD-DFT/6–31++G**) for the S_0-$S_1(B_{2u})$ and S_0-$S_2(B_{1u})$ vertical excitations and the S_1/S_2 minimum. b) Unrelaxed energy scans along the ν_8 A_g mode of the ground, S_1, S_2, D_0 and D_1 states.

that of an intermediate resonant excited state. For naphthelene, the situation is rather complex, as the S_1 state correlates with the D_0 (^2A_u, 8.14 eV) and D_1 ($^2B_{3u}$, 8.87 eV) ion states [22], which can be reached by the absorption of three 800 nm photons. As shown by Schmitt *et al.* [22] photoelectron bands corresponding to the D_0 and D_1 states are observed after internal conversion of the prepared S_2 state. Accordingly, we should consider the evolution of the ionization cross-section along both continua. Regarding the examined coordinates, the D_0 and D_1 surfaces are not parallel along the totally symmetric A_g modes, as the scans along the ν_8 A_g mode included in Fig. 4b show. In fact, it has been demonstrated that these modes induce numerous crossings among cationic states that develop in multiple Cis [40]. In this situation, we can conclude that it is plausible that the evolution of the S_1 state along the ν_8 A_g vibration causes the required modulation of the ionization probability necessary to observe the oscillation.

Concerning the low frequency oscillation (115 cm^{-1}), its origin was examined in a previous publication [24]. There, it was concluded that it could not be explained by wavepacket dynamics and it was attributed to electronic quantum beats (Rabi oscillations) caused by the coherent evolution of the coupled S_2/S_1 states. This explanation was sustained by the particular behavior exhibited by this oscillation, specifically: i) it is a damped oscillation that appears with the onset of the excitation and is not perceptible after three periods. ii) The oscillation frequency was observe to decrease with the excitation wavelength. iii) The frequency is lower than any of the normal modes predicted for the S_2 or S_1 states. Under this interpretation, despite most of the population relaxes to S_1 after the first beat, some of it remains in the upper state and the electronic coherence is maintained for longer times [16,24]. To the best of our knowledge, no other coherent oscillations of electronic nature have been reported for the non-adiabatic coupling of neutral electronic states in aromatic molecules. In order to check the plausibility of this assignation, calculations of the involved neutral and ionic PES along these low frequency modes would be required.

4. Conclusions

The carried out work demonstrates an efficient method to prepare sub-20 fs pulses at 264 nm by TH generation in the filament formed directly in the open atmosphere of the lab. With the simple set-up installed, resolutions ~25 fs are achieved in pump–probe experiments, where the temporal evolution of the prepared electronic excited state is tracked by multi-photon ionization. This pulse regime allows us to efficiently prepare wavepackets on individual targeted states of neutral molecules, which can be followed through coupling regions to provide detailed information on the non-adiabatic electronic-nuclear interaction. We have used the generated pulses to study the non-adiabatic relaxation the in highly symmetric PAH molecule of Naphthalene. The experiment has provided unprecedented detailed signals about the temporal evolution of the non-adiabatically coupled S_2/S_1 states of the molecule, after the initial excitation of the bright S_2 state. The transient shows oscillations that could be attributed to the coherent electronic evolution of the interacting states, together with faster beatings that correspond to the vibrational wavepacket propagation on the coupled potentials. By comparison with experimental and theoretical data, the observed faster oscillations are tentatively assigned to vibrational modes of the S_1 state. However, the rich observable retrieved invites to a rigorous modelling, which including the electronic degrees of freedom and the relevant nuclear coordinates, could provide more insights on the phenomenon.

CRediT authorship contribution statement

Álvaro Peralta Conde: Conceptualization, Methodology, Investigation, Writing – review & editing. **Iker Lamas:** Conceptualization, Methodology, Investigation, Writing – review & editing. **Marina Sánchez Albaneda:** Conceptualization, Methodology, Investigation. **Cruz Méndez:** Methodology, Investigation. **Asier Longarte:** Conceptualization, Methodology, Investigation, Writing – original draft, Project administration, Funding acquisition. **Raúl Montero:** Conceptualization, Methodology, Investigation, Writing – original draft.

Declaration of Competing Interest

The authors declare that they have no known competing financial interests or personal relationships that could have appeared to influence the work reported in this paper.

Data availability

Data will be made available on request.

Acknowledgements

All the experiments were carried out at the CLPU facility. The authors acknowledge the assistance from the CLPU technical and administrative personnel. They also thank the financial support from the Spanish MINECO through the grant: PGC2018-098561-B-C21. The work was also funded by the Basque Government (IT1162-19 and IT1491-22).

I. Lamas thanks the UPV/EHU for his predoctoral fellowship. Technical and human support provided by SGIker (UPV/EHU, MICINN, GV/EJ, ESF) is also gratefully acknowledged. The authors greatly appreciate the Open Access funding provided by University of Basque Country.

References

[1] *Conical Intersections: Theory, Computation & Experiment, World Scientific: Singapore*, ed. W. Domcke, D. R. Yarkony and H. Köppel, World Scientific, 2011.
[2] W. Domcke, D.R. Yarkony, Annu. Rev. Phys. Chem. 63 (2012) 325–352.
[3] C.h. Neidel, J. Klei, C.-H. Yang, A. Rouzée, M.J.J. Vrakking, K. Klünder, M. Miranda, C.L. Arnold, T. Fordell, A. L'Huillier, M. Gisselbrecht, P. Johnsson, M. P. Dinh, E. Suraud, P.-G. Reinhard, V. Despré, M.A.L. Marques, F. Lépine, Phys. Rev. Lett. 111 (2013), 033001.
[4] F. Calegari, D. Ayuso, A. Trabattoni, L. Belshaw, S. De Camillis, S. Anumula, F. Frassetto, L. Poletto, A. Palacios, P. Decleva, J.B. Greenwood, F. Martín, M. Nisoli, Science 346 (2014) 336.
[5] S.R. Leone, C.W. McCurdy, J. Burgdörfer, L.S. Cederbaum, Z. Chang, N. Dudovich, J. Feist, C.H. Greene, M. Ivanov, R. Kienberger, U. Keller, M.F. Kling, Z. Loh, T. Pfeifer, A.N. Pfeiffer, R. Santra, K. Schafer, A. Stolow, U. Thumm, M.J. J. Vrakking, Nature Photonics 8 (2014) 162–166.
[6] M. Nisoli, P. Decleva, F. Calegari, A. Palacios, F. Martín, Chem. Rev. 117 (2017) 10760–10825.
[7] Attosecond Molecular Dynamics, ed. M. J. J. Vrakking and F. Lepine, RSC, 2019.
[8] K. Kosma, S.A. Trushin, W. Fuss, W.E. Schmid, J. Phys. Chem. A 112 (2008) 7514–7529.
[9] T. Horio, T. Fuji, Y. Suzuki, T. Suzuki, J. Am. Chem. Soc. 131 (2009) 10392–10393.
[10] W.K. Peters, D.E. Couch, B. Mignolet, X. Shi, Q.L. Nguyen, R.C. Fortenberry, H. B. Schlegel, F. Remacle, H.C. Kapteyn, M.M. Murnane, W. Li, Proc. Natl. Acad. Sci. USA 114 (2017) 11072–11081.
[11] E.G. Champenois, L. Greenman, N. Shivaram, J.P. Cryan, K.A. Larsen, T. N. Rescigno, C.W. McCurdy, A. Belkacem, D.S. Slaughter, J. Chem. Phys. 150 (2019), 114301.
[12] D. Polli, P. Altoè, O. Weingart, K.M. Spillane, C. Manzoni, D. Brida, G. Tomasello, G. Orlandi, P. Kukura, R.A. Mathies, M. Garavelli, G. Cerullo, Nature 467 (2010) 440–443.
[13] T.A.A. Oliver, N.H.C. Lewis, G.R. Fleming, Proc. Natl. Acad. Sci. USA 111 (2014) 10061–10066.
[14] J. Brazard, L.A. Bizimana, T. Gellen, W.P. Carbery, D.B. Turner, J. Phys. Chem. Lett. 7 (2016) 14–19.
[15] J. Kim, C.H. Kim, C. Burger, M. Park, M.F. Kling, D.E. Kim, T. Joo, J. Phys. Chem. Lett. 11 (2020) 755–761.
[16] M. Seel, W. Domcke, J. Chem. Phys. 95 (1991) 7806–7822.
[17] A.V. Pisliakov, M.F. Gelin, W. Domcke, J Phys Chem A 107 (2003) 2657–2666.
[18] J. Krčmář, M.F. Gelin, W. Domcke, J. Chem. Phys. 143 (2015), 074308.
[19] K. Bennett, M. Kowalewski, S. Mukamel, J. Chem. Theory Comput. 12 (2016) 740–752.
[20] M. Kowalewski, B.P. Fingerhut, K.E. Dorfman, K. Bennett, S. Mukamel, Chem. Rev. 117 (2017) 12165–12226.
[21] L. Chen, M.F. Gelin, Y. Zhao, W. Domcke, J. Phys. Chem. Lett. 10 (2019) 5873–5880.
[22] M. Schmitt, S. Lochbrunner, J.P. Shaffer, J.J. Larsen, M.Z. Zgierski, A. Stolow, J. Chem. Phys. 114 (2001) 1206–1213.
[23] R. Montero, A. Longarte, R. Martínez, M.N. Sánchez Rayo, F. Castaño, Chem. Phys. Lett. 468 (2009) 134–137.
[24] R. Montero, Á.P. Conde, A. Longarte, F. Castaño, ChemPhysChem 11 (2010) 3420–3423.
[25] Y. Suzuki, T. Fuji, T. Horio, T. Suzuki, J. Chem. Phys. 132 (2010), 174302.
[26] L. Chen, M.F. Gelin, V.Y. Chernyak, W. Domcke, Y. Zhao, Faraday Discuss. 194 (2016) 61–80.
[27] S. Suntsov, D. Abdollahpour, D.G. Papazoglou, S. Tzortzakis, Opt. Express 17 (2009) 3190–3195.
[28] Y. Liu, C. Kou, A. Houard, A. Mysyrowicz, J. Opt. Soc. Am. B 36 (2019). G13–G18.
[29] A.T.J.B. Eppink, D.H. Parker, Rev. Sci. Instrum. 68 (1997) 3477–3484.
[30] R. Montero, V. Ovejas, M. Fernández-Fernández, Á. Peralta Conde, A. Longarte, J. Chem. Phys. 141 (2014), 014303.
[31] I. Lamas, A. Longarte, A. Peralta Conde, G. Muga, D. Townsend, R. Montero, J. Phys. Chem. A 123 (2019) 8982–8993.
[32] W. Fuß, W.E. Schmid, S.A. Trushin, J. Chem. Phys. 112 (2000) 8347–8362.
[33] M. J. Frisch, G. W. Trucks, H. B. Schlegel, G. E. Scuseria, M. A. Robb, J. R. Cheeseman, G. Scalmani, V. Barone, G. A. Petersson, H. Nakatsuji, X. Li, M. Caricato, A. V. Marenich, J. Bloino, B. G. Janesko, R. Gomperts, B. Mennucci, H. P. Hratchian, J. V. Ortiz, A. F. Izmaylov, J. L. Sonnenberg, D. Williams-Young, F. Ding, F. Lipparini, F. Egidi, J. Goings, B. Peng, A. Petrone, T. Henderson, D. Ranasinghe, V. G. Zakrzewski, J. Gao, N. Rega, G. Zheng, W. Liang, M. Hada, M. Ehara, K. Toyota, R. Fukuda, J. Hasegawa, M. Ishida, T. Nakajima, Y. Honda, O. Kitao, H. Nakai, T. Vreven, K. Throssell, J. A. Jr., J. E. Peralta, F. Ogliaro, M. J. Bearpark, J. J. Heyd, E. N. Brothers, K. N. Kudin, V. N. Staroverov, T. A. Keith, R. Kobayashi, J. Normand, K. Raghavachari, A. P. Rendell, J. C. Burant, S. S. Iyengar, J. Tomasi, M. Cossi, J. M. Millam, M. Klene, C. Adamo, R. Cammi, J. W. Ochterski, R. L. Martin, K. Morokuma, O. Farkas, J. B. Foresman and D. J. Fox, Gaussian16 Rev. A.03,Wallingford, CT, 2016.
[34] R.S. Mulliken, J. Chem. Phys. 23 (1955) 1997–2011.
[35] M. Rubio, M. Merchán, E. Ortí, B.O. Roos, Chem. Phys. 179 (1994) 395–409.
[36] P. Elliott, F. Furche and K. Burke, in Reviews in Computational Chemistry, Volume 26, ed. K. B. Lipkowitz and T. R. Cundari, John Wiley & Sons, Inc., 2008, pp. 91-165.
[37] S.M. Beck, D.E. Powers, J.B. Hopkins, R.E. Smalley, J. Chem. Phys. 73 (1980) 2019–2028.
[38] F. Negri, M.Z. Zgierski, J. Chem. Phys. 104 (1996) 3486–3500.
[39] K.F. Hall, M. Boggio-Pasqua, M.J. Bearpark, M.A. Robb, J. Phys. Chem. A 110 (2006) 13591–13599.
[40] A. Marciniak, V. Despré, T. Barillot, A. Rouzée, M.C.E. Galbraith, J. Klei, C. Yang, C.T.L. Smeenk, V. Loriot, S.N. Reddy, A.G.G.M. Tielens, S. Mahapatra, A.I. Kuleff, M.J.J. Vrakking, F. Lépine, Nature Communications 6 (2015) 7909.
[41] M. Stockburger, H. Gattermann, W. Klusmann, J. Chem. Phys. 63 (1975) 4519–4528.
[42] G.S. Jas, K. Kuczera, Chem. Phys. 214 (1997) 229–241.
[43] F.M. Behlen, S.A. Rice, J. Chem. Phys. 75 (1981) 5672–5684.